Harmful Algae 155 (2026) 103112

Contents lists available at ScienceDirect

Harmful Algae

journal homepage: www.elsevier.com/locate/hal

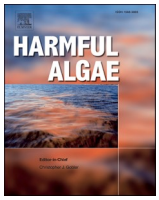

Cytotoxicity unleashed: how *Prymnesium parvum* extract drives RTgill-W1 rainbow trout cells into cell death

Zsuzsanna Neer [a,b], Endre Kiss [c], Urban Tillmann [d], Magdalena Pöchhacker [b,e,f], Balázs Vajna [a], Tamás Felföldi [g,h], János Matkó [i], Elisabeth Varga [b,*]

[a] *Department of Microbiology, Faculty of Science, Eötvös Loránd University, Pázmány Péter sétány 1/c 1117 Budapest, Hungary*
[b] *Unit Food Hygiene and Technology, Centre Food Science, Clinical Department Farm Animals and Food System Transformation, University of Veterinary Medicine, Vienna, Veterinärplatz 1 1210 Vienna, Austria*
[c] *BioOptics FACS Facility, Max Perutz Labs, Dr. Bohr-Gasse 9 1030 Vienna, Austria*
[d] *Section Ecological Chemistry, Alfred Wegener Institut-Helmholtz Zentrum für Polar- und Meeresforschung, Am Handelshafen 12, Bremerhaven D-27570, Germany*
[e] *Department of Food Chemistry and Toxicology, Faculty of Chemistry, University of Vienna, Währinger Str. 38-40 1090 Vienna, Austria*
[f] *Vienna Doctoral School in Chemistry (DoSChem), Faculty of Chemistry, University of Vienna, Währinger Str. 42 1090 Vienna, Austria*
[g] *Institute of Aquatic Ecology, HUN-REN Centre for Ecological Research, Karolina str. 29 1113 Budapest, Hungary*
[h] *National Multidisciplinary Laboratory for Climate Change, HUN-REN Centre for Ecological Research, Karolina Str. 29 1113 Budapest, Hungary*
[i] *Department of Immunology, Faculty of Science, Eötvös Loránd University, Pázmány Péter sétány 1/c 1117 Budapest, Hungary*

ARTICLE INFO

Keywords:
Microalgal toxins
Prymnesins
Flow cytometry
Fluorescence microscopy
Endpoint analysis

ABSTRACT

Massive algal blooms, including the 2022 Oder disaster linked to the toxic haptophyte *Prymnesium parvum*, highlight critical gaps in our understanding of waterborne ecotoxicants. Prymnesins are ladder-framed polyether-type compounds produced by *P. parvum* with well-documented ichthyotoxic properties; however, the cellular mechanisms underlying prymnesin-induced fish cell injury have yet to be resolved at the cellular level. Here, we establish and optimize molecular and cellular bioassays using fluorescence microscopy and flow cytometry to characterize early cell-damage pathways in rainbow trout gill cells (RTgill-W1) following a 3-hour exposure to a B-type prymnesin-containing algal extract. We specifically focused on cell death-associated events induced by *P. parvum* extract. Our endpoint analyses revealed a concentration-dependent shift in the dominant mode of cell death, with lower toxin levels predominantly triggering apoptosis, as indicated by nuclear morphological alterations, decreased mitochondrial mass, and phosphatidylserine externalization (Annexin V staining). In contrast, higher prymnesin concentrations induced necrotic cell death, characterized by membrane rupture and loss of cellular integrity as detected by propidium iodide uptake. By resolving concentration-dependent transitions between apoptotic and necrotic cell death, this study positions prymnesin-containing extracts as drivers of progressive intracellular injury rather than as agents exhibiting exclusively rapid membrane-lytic toxicity within the spectrum of macrocyclic polyether algal toxins. These findings highlight the dual nature of prymnesin-mediated cytotoxicity and demonstrate that exposure concentration is a critical determinant of cellular outcome, thereby advancing the mechanistic understanding of *P. parvum*-associated ichthyotoxicity. Beyond defining prymnesin-associated cytotoxicity during harmful algal blooms, the results indicate that fish gill epithelial cells initially engage in regulated stress responses at sublethal exposure levels, which may reflect early compensatory processes that modulate cellular tolerance.

1. Introduction

The increasing frequency of ecological disasters worldwide, driven by anthropogenic factors and climate change, has highlighted the fragility of aquatic habitats (Häder et al., 2020). Over recent decades, harmful algal blooms (HABs) caused by the rapid proliferation of aquatic photosynthetic microbes have occurred frequently in coastal waters and freshwater ecosystems worldwide, leading to massive fish mortality or severe ecological damage (Dai and Yang et al., 2023; Feng et al., 2024; Gobler, 2020; Griffith and Gobler, 2020). HABs often result

* Corresponding author.
E-mail address: elisabeth.varga@vetmeduni.ac.at (E. Varga).

https://doi.org/10.1016/j.hal.2026.103112
Received 18 August 2025; Received in revised form 26 February 2026; Accepted 27 March 2026
Available online 28 March 2026

from salinization, eutrophication, urbanization, climate change, altered hydrology, and agricultural runoff (Granéli et al., 2012; Hallegraeff, 1993; Hill et al., 2020; Paerl and Huisman, 2009; Roelke et al., 2011). In August 2022, a large-scale fish kill occurred in the Odra/Oder River (Poland/Germany), representing one of the most severe recent freshwater HAB-related ecological disasters in Europe and highlighting the potential consequences of *Prymnesium parvum* blooms (Köhler et al., 2024). The first recorded mass fish kills associated with *P. parvum* blooms date back to the 1920s in the Netherlands (Liebert and Deerns, 1920). Since then, numerous cases of fish mortality caused by this species have been reported worldwide (Edvardsen and Paasche, 1998), particularly in the United States, where recurring blooms occur (Baker et al., 2007). Multiple studies demonstrate that these microalgae produce toxins that kill gilled organisms in various ways. Their effects can be hemolytic, cytolytic, ichthyotoxic, or a combination of these (Roelke et al., 2007).

P. parvum is a unicellular microalga belonging to the Prymnesiaceae of the phylum Haptophyta, frequently termed "golden alga" due to the fucoxanthin pigments found in its chloroplasts (Berger et al., 1977; Edvardsen et al., 2011). Its ecological success largely reflects its broad tolerance to salinity and temperature, which enables growth across a wide range of environmental conditions (Baker et al., 2007).

Understanding the mechanisms underlying fish kills caused by *P. parvum* is key to explaining their impacts on both cultured and natural fish populations (Edvardsen and Paasche, 1998), which disrupt ecosystems and cause substantial economic losses (Southard et al., 2010). Toxins released by *P. parvum* can strongly affect co-occurring plankton, altering community structure (Fistarol et al., 2003) and influencing trophic interactions (Tillmann, 2003). These toxins are often collectively referred to as allelochemicals, as they contribute to competitive interactions by inhibiting co-occurring phytoplankton and facilitating prey capture. Fish mortality is generally considered a non-adaptive side effect of this chemical interference, which may be enhanced under suboptimal growth conditions. (Granéli and Hansen, 2006; Granéli and Salomon, 2010; Legrand et al., 2003). The toxins produced by *Prymnesium parvum* are considered chemically diverse, and over the years, multiple compound classes have been proposed as candidates (Bertin et al., 2012; Dafni et al., 1972; Henrikson et al., 2010; Kozakai et al., 1982). However, for most of these compounds, definitive structural elucidation is lacking.

By contrast, ladder-frame polyether prymnesins were unequivocally identified as the primary ichthyotoxic metabolites of *P. parvum* (Igarashi et al., 1995, 1996, 1999; Rasmussen et al., 2016). First isolated as prymnesin-1 and −2 in 1995, this toxin family has since expanded to include additional congeners, such as prymnesin-B1, which exhibits subtle structural variations (Rasmussen et al., 2016). Detecting prymnesins is technically demanding because of their nanomolar potency and low cellular abundance, and they are thought to be released primarily during prey encounters or under physical stress (Remmel et al., 2012).

Fish gills are continuously exposed to waterborne toxicants and serve as the main interface between the aquatic environment and the internal physiology of fish. In addition to gas exchange, gills play essential roles in ion transport, acid–base regulation, osmoregulation, and excretion of metabolic byproducts (McKim et al., 1985; Wood et al., 2002). Gill epithelial cells have been shown to be more sensitive to environmental toxins than hepatocytes in freshwater fish (Zhou et al., 2006). Although primary gill cell cultures closely resemble in vivo function, the use of immortalized gill cell lines such as RTgill-W1 offers practical advantages, including reduced variability and improved reproducibility (Bols et al., 1994).

Upon toxic exposure, apoptosis in gill epithelial cells likely represents an early protective response by maintaining epithelial integrity and limiting inflammatory damage associated with necrosis (Chen et al., 2023; Sales et al., 2017). Regulated cell death is a key cellular endpoint for assessing gill responses to aquatic toxins.

Identifying cells undergoing apoptosis can be challenging because many assays are used to detect structural and functional changes that may also occur in other cellular processes. Additionally, no single parameter can fully define programmed cell death across all systems, and these morphological changes can vary with apoptotic pathways or cell types. For this reason, a multi-parameter approach combining several complementary assays is required. In this study, substantial optimization and validation were therefore necessary for the fluorescence microscopy and flow cytometry protocols implemented during assay development for the trout gill cell line.

Despite extensive documentation of fish kills associated with *Prymnesium parvum* blooms, the cellular mechanisms underlying prymnesin-induced toxicity remain poorly characterized. By comparison, several other HAB-associated ichthyotoxins have been investigated in considerable mechanistic detail. For example, karlotoxins form sterol-dependent membrane pores (Place et al., 2024), brevetoxins primarily target voltage-gated sodium channels (Baden et al., 2005), and raphidophyte-derived toxins are frequently linked to oxidative stress–mediated pathways (Kim et al., 2000). These studies illustrate that macrolide polyether algal toxins comprise multiple, structurally and functionally diverse toxin families with distinct modes of action. At present, a comparable cellular-level mechanistic framework is lacking for prymnesins. This leaves open the question of how prymnesin-induced cellular responses relate to the described ichthyotoxin pathways, or whether they represent a new mode of intracellular injury.

Addressing this gap is critical for linking ecological observations of *P. parvum*–associated fish mortality to underlying cellular processes. Thus, our study aimed to characterize the cell death-inducing effects of *P. parvum* extract in RTgill-W1 cells by examining alterations in plasma membrane integrity, cellular and nuclear morphology, cell-surface exposure of phosphatidylserine (PS), mitochondrial mass, and lysosomal activity.

2. Materials and methods

2.1. Prymnesium parvum cultivation and toxin extraction

The *P. parvum* strain used (KD-A4) was isolated from water samples collected from the Oder River at the end of the summer 2022 bloom (52.887° N, 14.159° E). Cultivation took place in a 10 L glass bottle under non-axenic conditions at 20 °C with a light:dark cycle of 16:8 h (30–40 µmol photons m^{-2} s^{-1}) and constant, gentle bubble aeration. Filter-sterilized K-medium (Keller et al., 1987) based on natural North Sea water, adjusted to a salinity of 15, served as a growth medium. The algal biomass was harvested in the late exponential phase of the *P. parvum* culture (cell density of 0.69×10^6 cells mL^{-1}) by centrifugation of 6 × 1 L culture at 8000 x *g* for 20 min at 15 °C, and the biomass pellet was separated from the supernatant. The pellets were combined and stored at −20 °C until extraction, following the protocol of Binzer et al. (2019). First, the algal cell pellet was thawed, then centrifuged at 3220 x g for 10 min to remove any remaining supernatant. Second, the pellets were extracted several times with ice-cold acetone to remove chlorophyll until a light green supernatant was obtained (centrifugation at 4080 x *g*, 15 min, 4 °C). Third, prymnesins were subsequently extracted with methanol (MeOH). The MeOH was then evaporated with a CentriVap Benchtop Vacuum Concentrator coupled to a CentriVap Coldtrap (both Labconco Corp., Kansas City, MO, USA), and the samples were reconstituted in absolute ethanol (EtOH). Finally, the samples were placed in an ultrasonic bath for several minutes, centrifuged, and the particle-free supernatant was transferred to glass sample vials and stored at −20 °C.

2.2. Prymnesin profile

The prymnesin profile was analyzed using ultra-high-performance liquid chromatography coupled to high-resolution mass spectrometry

(UHPLC—HRMS), as described by Varga and Prause et al. (2024). The only difference was that a Vanquish HPLC-System coupled to an Orbitrap Q Exactive Plus (both Thermo Fisher Scientific, Waltham, MA, USA) was used for detection. Data evaluation was performed with FreeStyle 1.8 SP2 and Skyline 23.1.0.268. Toxin concentrations in prymnesin samples were estimated by high-performance liquid chromatography with fluorescence detection (HPLC-FLD), as previously described (Svenssen et al., 2019). In short, prymnesins were labelled with a fluorescent tag (AccQ-Tag Fluor Reagent Kit, Waters Corp., Milford, MA, USA) through derivatization of their primary amines. A 1200 HPLC system (Agilent Technologies, Waldbronn, DE), using an Agilent Poroshell C18 column (2.1 × 50 mm, 2.7 μm) with water as eluent A and acetonitrile as eluent B, both containing 0.1 % formic acid, were used for chromatographic separation. Prymnesins were detected via fluorescence at excitation/emission wavelengths of 250/395 nm. The data were analyzed using ChemStation for LC Rev. B.04.01 SP1 (Agilent Technologies).

2.3. Fish gill cell culture

The assays were performed with the rainbow trout-derived gill cell line RTgill-W1 obtained from Kristin Schirmer (Department of Environmental Toxicology, EAWAG, Dübendorf, CH). The RTgill-W1 cell line is an immortal cell line originally developed from a primary cell culture established from pieces of gill filaments of rainbow trout *(Oncorhynchus mykiss)* (Bols et al., 1994). The gill cell line was cultured at 19 °C in Leibovitz's/ L-15 (Gibco, Grand Island, NY, US) medium supplemented with 10 % FBS (*v/v*) and 1 % PenStrep (Gibco, Grand Island, NY, US) according to the manufacturer's instructions, and sub-cultured every week, by first rinsing the flask with Versene (Thermo Fisher Scientific, Waltham, MA, US) and subsequent trypsinization using 0.25 % trypsin/0.02 % ethylenediaminetetraacetic acid in phosphate-buffered saline (PAN Biotech, Aidenbach, Germany).

The cell line was cultured in cell culture flasks using the "cell + surface" (Sarstedt AG & Co KG, Nürnbrecht, Germany) of diverse sizes (T-25 to T-75). The assays were performed in 96-well polystyrene cell culture plates (cell + surface, flat base, order number 83.3924.300; Sarstedt AG & Co. KG, Nürnbrecht, Germany) for CellTiter-Blue, in μ-Slide ibiTreat 8-well high wall chamber slides (#1.5 polymer coverslip, tissue culture treated; Ibidi GmbH, Gräfeling, Germany #80,806) for live-cell imaging, or in 5 mL round-bottom test tubes (Corning) for flow cytometry.

2.4. Cell viability assays

Cell viability was assessed using both a metabolic assay and morphological analyses. The CellTiter-Blue® (CTB) assay was performed as a 1-hour endpoint measurement, initiated at the 3rd hour of toxin exposure and completed at the 4th hour. This assay measures the conversion of resazurin to resorufin by metabolically active cells, with fluorescence intensity correlating to overall viability. In parallel, real-time viability was monitored using live-cell microscopy and flow cytometry (FACS). Cells were stained with appropriate live/dead fluorescent markers (propidium iodide) and analyzed to distinguish between viable and apoptotic/necrotic populations.

RTgill-W1 cells were seeded at 20,000 cells/well in 96-well plates and cultured for 48 h. PRM samples in EtOH were diluted 1:2000 in a culture medium. Since PRMs are light-labile, exposure to sunlight was avoided, and the exposure time to artificial light was kept to a minimum. Cells were exposed to 100 μL of diluted *P. parvum* extract at different concentrations for 3 h in the dark.

The CTB assay (Promega Corporation, Vienna, Austria) was performed to measure cell metabolic activity according to the manufacturer's instructions. Each concentration was dosed in triplicate. Likewise, triplicates were used for the solvent control (0.1 % EtOH). The three wells without cells served as controls to detect potential background fluorescence from the test chemicals. After 3 h of incubation, the medium was replaced with a 1:10 (*v/v*) dilution of CTB dye in the cell culture medium and incubated for an additional hour in the dark. The EC_{50} was calculated with R version 4.5.0 and RStudio (version 2024.12.1) using the packages "misty" (https://cran.r-project.org/web/packages/misty/index.html), "drc" (https://cran.r-project.org/web/packages/drc/index.html), and "ggplot2" (https://cran.r-project.org/web/packages/ggplot2/index.html).

For the flow cytometry-based viability assay, RTgill-W1 cells were treated with *P. parvum* extract at various concentrations or with 0.1 % EtOH (solvent control). Half an hour before the end of the 3 h incubation, the dyes (Hoechst 33342 (4 μg/mL) and propidium iodide (PI) (0.8 μg/mL)) were added to the incubation solutions, and incubation continued for the remaining 30 min at 19 °C in the dark. Analysis was performed immediately thereafter with a BD LSRFortessa™ flow cytometer (BD Biosciences, San Jose, CA, USA). Hoechst staining was applied to exclude cellular debris from the analysis. Single-cell events were identified based on FSC-Area vs. FSC-Height parameters. To assess cell viability, the abundance of the PI-positive fraction, representing the dead-cell population with impaired plasma membrane integrity, was quantified.

2.5. Cell treatments and flow cytometry

Cells were plated into 25 cm^2 or 75 cm^2 flasks at densities of 0.5×10^6 or 1×10^6 cells, respectively, and allowed to attach and acclimate for 48 h before chemical exposure. Thereafter, the cells were trypsinized, resuspended in serum-free L-15/ex medium, and approximately 5×10^4 gill cells for each treatment group were transferred to sterile 1.5 mL Eppendorf tubes. The algal toxin dissolved in EtOH was diluted in L-15/ex solution to final concentrations of ~half of the EC_{50} (sublethal), ~EC_{50}, and ~five times the EC_{50} (lethal). To ensure solvent control, 0.1 % EtOH was used throughout all experiments, and the total volume was 800 μL across all treatments. These concentrations were based on preliminary range-finding experiments that established a dose-response for cell injury (see 2.4). All experimental treatments were conducted in serum-free L-15/ex solution (Schirmer et al., 1997). After 2.5 hours of incubation, the dyes were added to the cells and incubated for 30 min at 19 °C in the dark.

Sample acquisition was performed using a BD LSRFortessa™ flow cytometer (BD Biosciences, San Jose, CA, USA) having a 405/488/561/640 nm laser configuration, equipped with a high-throughput sampler unit and with BD FACSDiva™ software (BD Biosciences, San Jose, CA, USA). A total of five thousand events were acquired for each sample. Three independent experiments were performed for each sample. The data files were analyzed using the FlowJo™ v10.10.0 Software (BD Life Sciences, Ashland, OR, USA).

2.6. Cell treatments and confocal laser scanning microscopy

For confocal microscopy, 20,000 gill cells/well were plated in μ-Slide ibiTreat 8-well slides (Ibidi GmbH, Gräfeling, Germany #80,806) and allowed to adhere for 72 h. After removing the medium, the algal toxin extract dissolved in EtOH was diluted in L-15/ex solution to final concentrations of ~half of the EC_{50} (sublethal), ~EC_{50}, and ~five times EC_{50} (lethal). To control solvent effects, 0.1 % EtOH was used throughout all experiments, and each condition was dosed in triplicate. Treatment of the cells was conducted in an incubator (19 °C, standard atmosphere, in the dark). After 2.5 h, the dyes were added separately or in appropriate combinations, and incubation continued for an additional 30 min under the same conditions, for a total incubation time of 3 h. Each experiment was conducted at least three times, using cells from different passages, starting on different days, and employing freshly prepared chemical test solutions, thereby yielding a minimum of three biological replicates.

Image acquisition was performed with a Zeiss LSM 880 confocal

laser-scanning microscope (Zeiss, Jena, Germany) equipped with laser diode 405 nm, Argon 488 nm, DPSS 561 nm, and HeNe 633 nm lasers, ZEN 2 Black edition image acquisition software, and 10x/0.45 Plan-Apochromat, 20x/0.8 Plan-Apochromat, and 40x/1.40 Plan-Apochromat Oil DIC III objectives. Fluorescence image analysis and quantification of fluorescence intensity changes were performed using Fiji/ImageJ 1.54 (https://imagej.net/Fiji/Downloads). For intensity measurements, regions of interest (ROIs) were defined around single cells using a consistent workflow across conditions.

Confocal z-stack images of cell nuclei were subjected to three-dimensional reconstruction and quantitative analysis using Huygens Professional v25.4 (Scientific Volume Imaging, Hilversum, The Netherlands) (Supplementary Fig. S1). Before analysis, all images were anonymized and randomly renamed. Automated object detection and segmentation were performed using identical parameter settings for all samples. Nuclear volume distributions and morphology-based classifications were derived from the reconstructed datasets and used for downstream statistical evaluation.

2.7. Analysis of Prymnesium parvum extract-induced changes in forward angle and side light scattering properties of the cells

Cells undergoing apoptosis or necrosis show distinct physiological and morphological characteristics, which can be readily measured by flow cytometry (Darzynkiewicz et al., 1992; Tomer et al., 1988) via the cell's light scattering properties. The forward scatter (FSC) parameter is a measure of cell diameter/size, while the side scatter (SSC) signal reflects intracellular complexity/density (Darzynkiewicz et al., 1992). One morphological characteristic of early apoptosis is cellular shrinkage reflected by a decrease in the FSC signal (Darzynkiewicz et al., 1992). Because membrane integrity is not compromised in early apoptosis, the SSC signal either remains unchanged or increases due to chromatin condensation or mitochondrial swelling. When apoptosis is more advanced, the side scatter signal is also decreased. Late apoptotic cells are characterized by low forward- and side scatter signals (Pozarowski et al., 2003). In contrast to apoptotic cells, necrotic cells display plasma membrane rupture and cytosolic leakage, resulting in markedly diminished forward- and side scatter (Pozarowski et al., 2003).

Accordingly, the effect of *P. parvum* extract on cell morphology was investigated by monitoring the FSC and SSC properties of treated cells relative to those of ethanol-treated cells (solvent control) using flow cytometry. Briefly, a gate called 'region [1]' was drawn around the main cell population on the FSC/SSC bivariate dot plot based on the solvent control sample. To assess shifts in FSC and SSC of *P. parvum* extract-treated cell populations relative to this gate established for the control cell population, a second gate, defined as `region [2]´, was placed on the `FSC low/SSC low-to-high' part of the dot plot.

2.8. Flow cytometric analysis of cellular NAD(P)H levels at various stages of apoptosis

NAD(P)H autofluorescence (Minet et al., 2004) was measured in conjunction with other indicators via flow cytometry using a BD LSRFortessa flow cytometer with 405 nm (violet) excitation. The resulting blue fluorescence emission signal was collected using a 450/50 nm band-pass filter.

2.9. Mitochondrial mass analysis

Mitochondrial mass changes upon toxin treatment were analyzed by triple staining with 10-N-nonyl-acridine orange (NAO) (Biotium, Hayward, CA, US), Hoechst 33342 (4 μg/mL), and propidium iodide (0.8 μg/mL) via confocal microscopy. The NAO stock solution was prepared in DMSO according to the manufacturer's instructions, diluted with L-15/ex solution, and added to cells to reach a final concentration of 200 nM, followed by 30 min of incubation at 19 °C in the dark. Fluorescence imaging was performed with a Zeiss LSM 880 confocal laser scanning microscope. Images were processed with ZEN software (Zeiss). For fluorescence signal intensity estimation and data extraction, Fiji/ImageJ 1.54 was used.

2.10. Lysosome staining

LysoTracker Red DND-99 is a hydrophobic weak base and a fluorescent marker, which selectively accumulates in acidic vesicular compartments, predominantly in late endosomes and lysosomes. This probe exhibits an excitation maximum at 576 nm and an emission maximum at 590 nm. Remarkably, owing to the acidic pH of the lysosome, upon entry into the lysosome, LysoTracker Red becomes protonated and, hence, is markedly sequestrated in lysosomes. Moreover, because lysosomal acidity is crucial for the accumulation of LysoTracker within this organelle, its fluorescence intensity may indicate alterations in lysosomal pH (Zhitomirsky et al., 2018).

Cells (20,000 per well) were seeded and treated with *P. parvum* extract solutions as described before in μ-Slide ibiTreat 8-well chamber slides. LysoTracker® Red DND-99 (Invitrogen™, Thermo Fisher Scientific, Waltham, Massachusetts, USA) at a 50–75 nM dilution and Hoechst 33342 (4 μg/mL) were added to the cells and incubated for 30 min under the previously described cell culture conditions, protected from light. Stained samples were imaged with a Zeiss LSM 880 confocal microscope (10 × and 20 × objectives and 40 × oil objective).

Flow cytometric analysis of LysoTracker fluorescence was performed using 561 nm excitation and with a 586/15 nm emission bandpass filter with a BD LSRFortessa™ flow cytometer (BD Biosciences, San Jose, CA, USA).

2.11. Statistical analysis

Data are derived from at least three independent experiments and expressed as mean ± SEM. Statistical analysis was performed using the Kruskal-Wallis test with Dunn's multiple comparisons test in BioRender (https://BioRender.com) and Graphpad Prism v6.07 (Graphpad, La Jolla, CA, USA). *P* values of <0.05 were considered statistically significant. Statistical graphs were created using BioRender (https://BioRender.com) and Graphpad Prism v6.07.

3. Results

3.1. Prymnesium parvum extract strongly alters the viability of rainbow trout gill cells

A B-type PRM extract (KD-A4) was analytically characterized before the toxicity experiments. With the HPLC-FLD method described above, a prymnesin concentration of 181 ± 16 μM was estimated, and LC-HRMS determined the prymnesin composition. It revealed the presence of the B-type prymnesin backbone with one incorporated chlorine, as well as the analogue with pentose, hexose, or two hexose units (see Supplementary Table S2 for details). The fish gill cell line RTgill-W1 was exposed to this extract, and following an incubation time of 3 h, cell viability was assessed by CTB. Approximately 50 % cytotoxicity was achieved at a 1:10,000 dilution, corresponding to a prymnesin concentration of 18.1 nM.

To evaluate cell viability, both metabolic and morphological approaches were applied. The CellTiter-Blue (CTB) assay reflects only metabolic activity; it does not distinguish between different modes of cell death. By contrast, real-time live-cell imaging and flow cytometry (FACS)–based viability assays provide dynamic, high-resolution analysis using fluorescent markers to differentiate between live, apoptotic, and necrotic cells (Fig. 1). This complementary use of assays enables a more comprehensive evaluation of cellular responses to toxic exposure.

Treatment of RTgill-W1 cells with an EC_{50} concentration of *P. parvum* extract led to a substantial reduction in cell adherence to culture dishes.

Cell viability was assessed by flow cytometry. Fig. 1 shows the response of PI-staining in rainbow trout cells as a measure of cell viability to different concentrations of *P. parvum* extract. The frequency of late apoptotic and necrotic cells, characterized by loss of membrane integrity and thus by PI-positive staining, is summarized in Fig. 1C. *P. parvum* extract caused a dose-dependent increase in the fraction of PI-positive cells relative to the EtOH control. Statistically significant effects were observed only at the EC_{50} and the highest exposure concentration. In the 3-h time frame of the measurement, 7.2 % of the solvent-control-treated cells showed PI positivity. In the EC_{50}-treated cell sample, 34.7 % of the cells were PI-positive; hence, >50 % of cells remained viable after 3 h of treatment.

3.2. *Prymnesium parvum extract significantly changes nuclear morphology and induces chromatin condensation of RTgill-W1 cells*

Morphological hallmarks of apoptosis in the nucleus (Panel 1) are chromatin condensation and/or nuclear fragmentation. The morphological changes of nuclei in RTgill-W1 rainbow trout cells induced by different concentrations of *P. parvum* extract are shown in Fig. 2. The cells treated with the lethal dose and the solvent control were relatively uniform. In contrast, the EC_{50} and sublethal-treated samples appeared more heterogeneous; therefore, more nuclei were analyzed. After 3 h of incubation with the EC_{50} concentration, <10 % of the nuclei showed uncondensed/normal morphology. Compared with EC_{50}-treated cells, the percentage of condensed nuclei was lower at the sublethal dose. At higher extract concentrations, a greater number of cells exhibited chromatin condensation that initiated at the nuclear periphery and formed crescent- or ring-like structures.

Nuclear morphology was quantified using a fully anonymized and blinded image-analysis workflow in Huygens Professional. Image stacks were exported without treatment identifiers, randomly renamed, and processed using identical automated detection parameters. Treatment group results were revealed only after scoring was completed, ensuring an unbiased, reproducible, and investigator-independent analysis.

To compare nuclear volume distributions quantitatively (Supplementary Fig. S1), VoxVol values were grouped into four size-based categories: condensed (<450 voxel units), intact (450–900 voxel units), early damage (900–1400 voxel units), and fragmented (>1400 voxel units). Solvent control-treated cells (SC) showed a dominant population of intact nuclei (62 %), with approximately 10 % classified as condensed. By contrast, a dose-dependent shift toward smaller nuclear volumes was observed with increasing extract concentration. The condensed fraction increased to 22 % at sublethal exposure, 32 % at the EC_{50}, and nearly 70 % at lethal exposure. Early-damage (swollen) and fragmented nuclei remained minor populations but exhibited treatment-dependent increases. Across exposure levels, this size-based classification showed a clear shift from intact to compacted or condensed nuclear morphologies with increasing toxin load.

3.3. *Flow cytometric analysis of cellular NAD(P)H level modulated by Prymnesium parvum extract*

Fish gill cells contain endogenous fluorescent molecules, including aromatic amino acids, flavins, and the reduced pyridine nucleotides NADH and NADPH. Excitation of NAD(P)H at ~360 nm yields a fluorescent emission peak at 450 nm (blue) (Cano et al., 2008; Laing et al., 1980; Masters et al., 1989). Even though NAD(P)H molecules are fluorescent, the oxidized forms of NAD(P)H (NAD^+ and $NADP^+$) lose their fluorescence characteristics (Laing et al., 1980). Under these conditions, changes in NAD(P)H autofluorescence reflect alterations in cellular pyridine nucleotide redox status (Laing et al., 1980; Masters et al., 1989). A significant decrease in NAD(P)H autofluorescence was observed in the RTgill-W1 cells at EC_{50} and the lethal doses of *P. parvum* extract (Fig. 3A). At the EC_{50} concentration, incubation with *P. parvum* extract led to a 20 % decrease in NAD(P)H autofluorescence compared to the solvent control. A 50 % reduction was observed at the higher toxin concentration, resulting in acute cell death (Fig. 3B).

3.4. *Effect of Prymnesium parvum extract on forward angle and side light scatter properties of gill cells*

Treatment of the RTgill-W1 cells with increasing concentrations of *P. parvum* extract led to a gradual decrease in the FSC signal, indicating cellular shrinkage (Fig. 3C). In parallel, the cell population shifted into the SSC low-to-high region as cell death progressed. As illustrated in Fig. 3D, exposure to a *P. parvum* extract at half of the EC_{50} (= sublethal) caused a moderate decrease in the FSC signal, accompanied by an increase in SSC. Treatment with the EC_{50} dose results in a further decline in the FSC signal and a significant increase in the SSC signal. At the lethal concentration, the majority of the cells (90.5 %) fell within the gated area characterized by low FSC signals and a wide range of SSC signals.

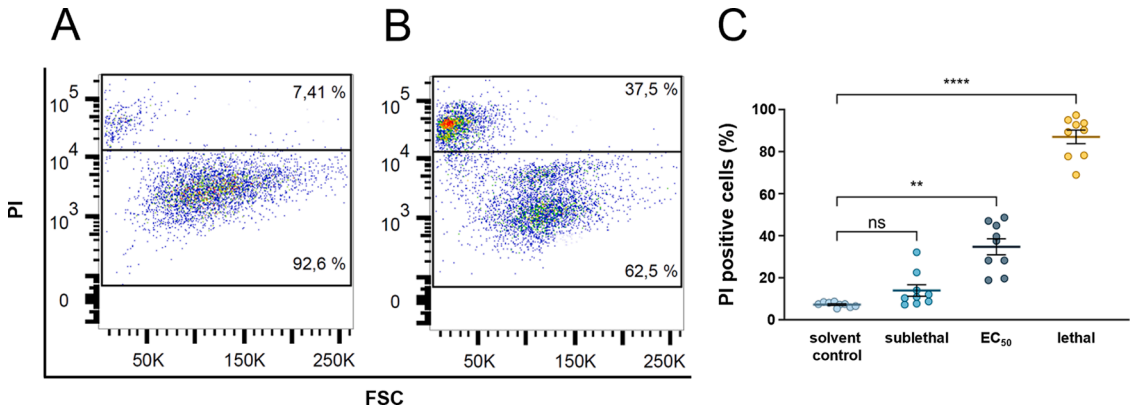

Fig. 1. Effects of *P. parvum* extract on cell viability assessed by flow cytometric analysis of propidium iodide (PI) uptake. RTgill-W1 cells were treated for 3 h with solvent control or *P. parvum* extract, followed by PI staining and flow cytometric analysis. Cells with compromised plasma membrane integrity were identified based on PI positivity. Representative flow cytometry dot plots show PI-negative and PI-positive cell populations following treatment with the solvent control (A) or *P. parvum* extract at the EC_{50} concentration (B). Quantification of PI-positive cells is shown in panel (C) as mean percentage ± SEM from three independent experiments, each performed with three technical replicates. Statistical differences between extract-treated samples and the solvent control were analyzed using the Kruskal–Wallis test followed by Dunn's multiple comparisons test (**$p < 0.01$; ****$p < 0.0001$; ns, not significant). FSC, forward scatter; SEM, standard error of the mean. Created in BioRender. Neer, Z. (2026) https://BioRender.com/zmh8z18.

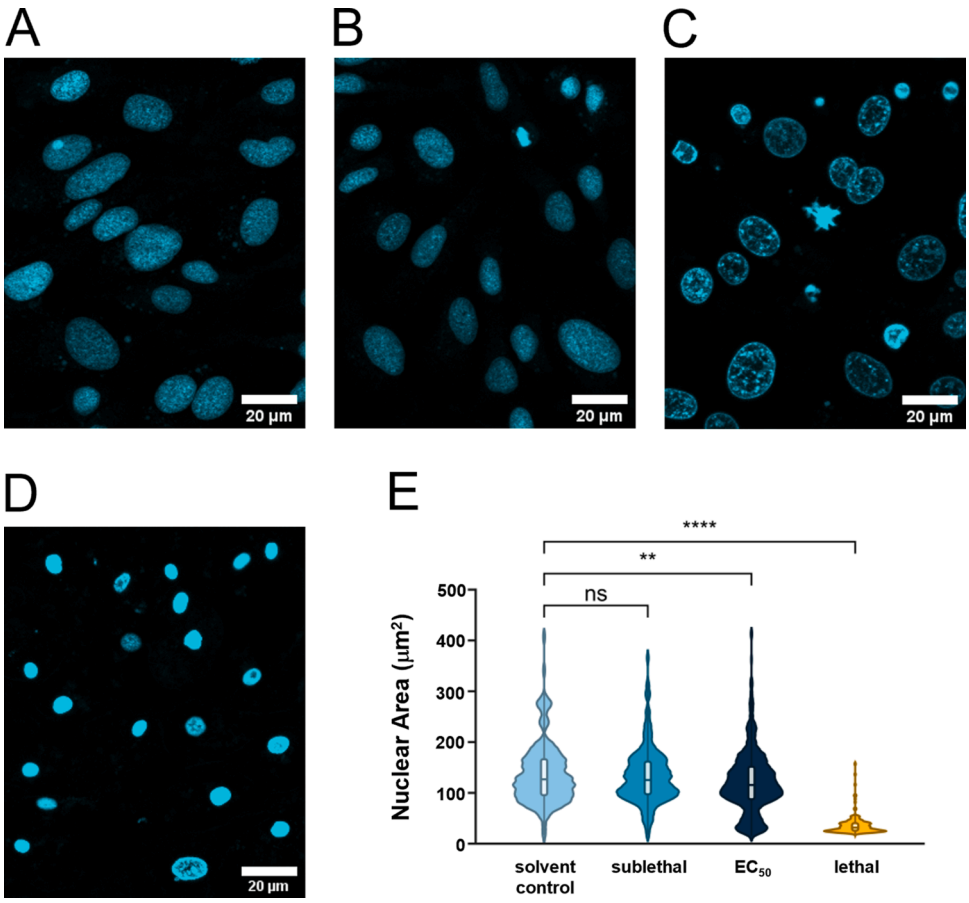

Fig. 2. Effect of *P. parvum* extract on nuclear morphology of RTgill-W1 cells. Representative images of nuclei of RTgill-W1 cells dosed with solvent control (A) or with *P. parvum* extract (B: sublethal, C: $EC_{50,}$ and D: lethal concentration) for 3 h. Cell nuclei were subsequently stained with Hoechst 33342 (cyan blue) and visualized by confocal microscopy. Representative fluorescence microscopy images with Hoechst 33342-stained nuclei from the untreated/*Prymnesium* extract-treated cell populations. The nuclear area was quantified by Fiji software. The violin plots (E) present the statistical analysis of measured nuclear areas. Number of cells analyzed: $n = 185$ (solvent control); $n = 358$ (sublethal); $n = 669$ (EC_{50}); $n = 175$ (lethal). Asterisks represent significant differences between the *P. parvum* extract-treated samples and the solvent control, analyzed by Kruskal-Wallis non-parametric test with Dunn's multiple comparisons test (** $p < 0.01$; **** $p < 0.0001$). Not significant difference: ns. Created in BioRender. Neer, Z. (2026) https://BioRender.com/zmh8z18.

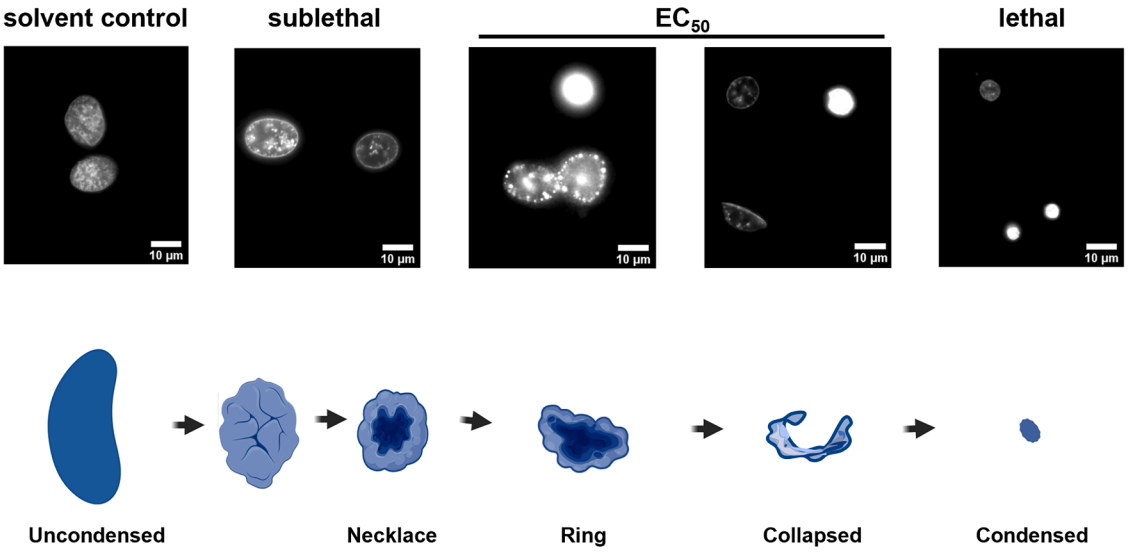

Panel 1. Classification of progressive apoptotic stages based on chromatin morphology. Apoptotic cell death is characterized by a series of morphological changes, including chromatin condensation. Condensation initiates at the nuclear periphery and progresses along the nuclear membrane, forming a necklace- or ring-like pattern, and ultimately leading to a highly compacted chromatin body associated with nuclear shrinkage. The images illustrate successive stages of chromatin condensation and nuclear remodeling. Representative fluorescence microscopy images show Hoechst 33342–stained nuclei of RTgill-W1 cells from untreated and *Prymnesium* extract–treated populations. Created in BioRender. Neer, Z. (2026) https://BioRender.com/zmh8z18.

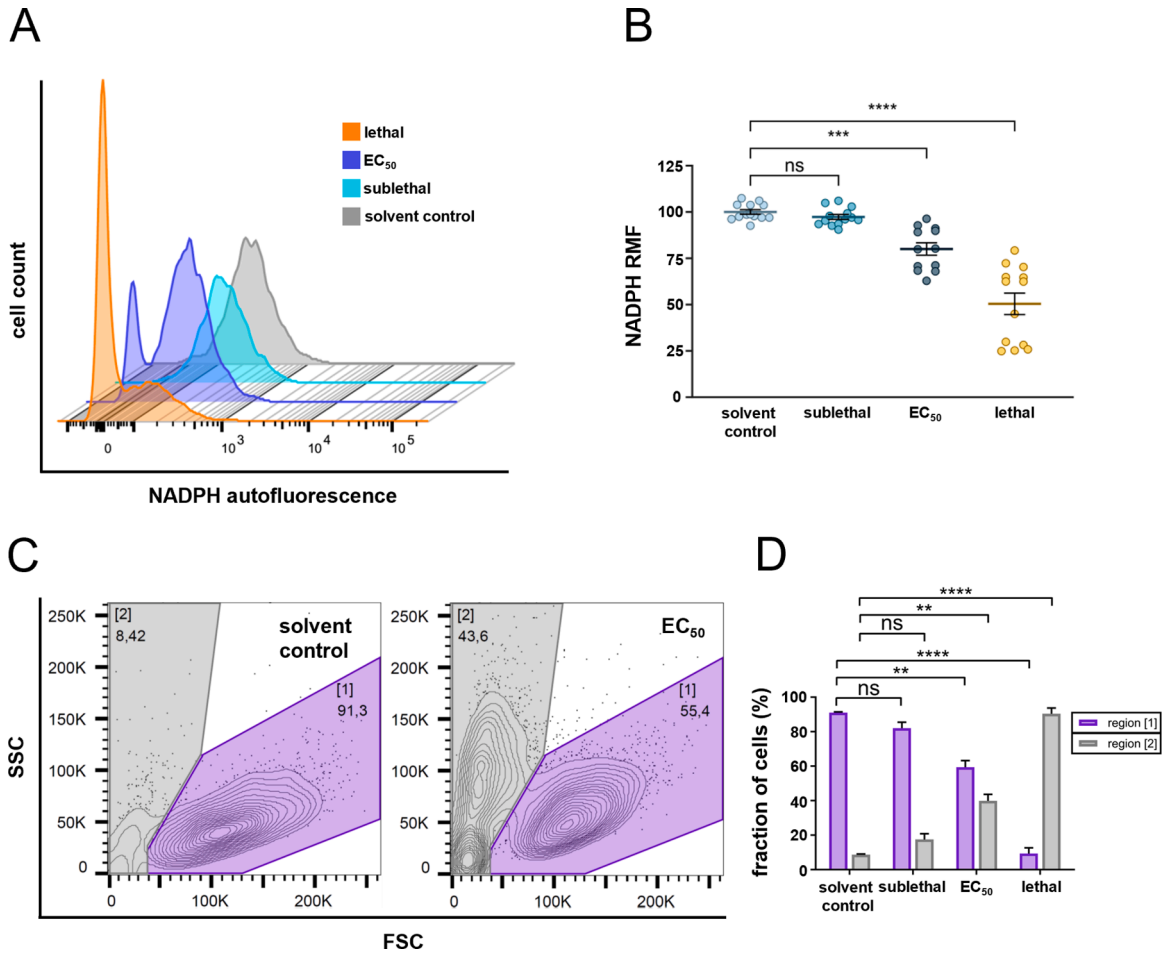

Fig. 3. NAD(P)H autofluorescence and light scatter characteristics of RTgill-W1 cells following exposure to *P. parvum* extract.
Panel A, B: RTgill-W1 cells treated with solvent control or with *P. parvum* extract for 3 h. Cellular NAD(P)H content was quantified as the cells' autofluorescence, measured at an excitation wavelength of 405 nm and emission wavelengths of 425–475 nm. The histogram analysis (A) depicts the NAD(P)H autofluorescence intensity distribution in the solvent control (grey) and *P. parvum* extract-treated samples at sublethal (cyan), EC_{50} (blue), and lethal (orange) doses. Panel B represents the relative mean fluorescence (RMF) of NAD(P)H autofluorescence intensity normalized to the solvent control ± SEM.
Panels C, D: Representative flow cytometry contour plots (C) demonstrating the morphological changes of RTgill-W1 cells based on forward scatter (FSC, ~ cell size) and side scatter (SSC, ~ internal granularity) parameters after 3 h of *P. parvum* extract treatment. Cell subpopulations appearing in FSC-SSC region [1] (purple color, normal cell size and granularity) vs. region [2] (grey color, FSC-low/SSC low-to-high cells) were quantified and plotted on the bar graph (D) showing the fraction of cells (%) within the two subpopulations ± SEM.
Statistical significance was determined using the Kruskal–Wallis test followed by Dunn's multiple comparisons test (** $p < 0.01$; *** $p < 0.001$; **** $p < 0.0001$; ns: not significant). Created in BioRender. Neer, Z. (2026) https://BioRender.com/zmh8z18.

3.5. *Prymnesium parvum extract induces phosphatidylserine redistribution in the plasma membrane of gill cells*

Apoptosis progression was monitored using Annexin V-FITC and PI staining. Changes in the cell membrane are observed throughout the apoptotic process at the EC_{50}, indicating distinct stages in the cell population. Distortion or blebbing of the cell membrane, as well as changes in membrane integrity, were detectable as indicators of apoptotic progression. One such change is the translocation of the phospholipid phosphatidylserine (PS) from the intracellular leaflet of plasma membrane to the extracellular side (Fig. 4). Annexin V is a phospholipid-binding protein with a strong affinity for PS. For this reason, fluorescently labelled Annexin V (Annexin V-FITC) can be used to detect exposed PS on the cell surface, directly identifying early apoptotic events. In contrast, PI highlights cells with loss of membrane integrity, thereby facilitating distinction between early apoptotic and late apoptotic or necrotic populations (van Genderen et al., 2006).

The Annexin V positivity of EC_{50}-treated RTgill-W1 cells exceeded 30.2 % ($n = 179$). In the control cell population, 2.0 % of the cells were early apoptotic after 3 h of incubation, while 3.0 % of cells treated with a sublethal concentration showed early signs of apoptosis. In the lethal treatment group, 100 % of cells exhibited signs of disruption, and only cell membrane remnants or necrotic cells were visible by microscopy.

3.6. *Prymnesium parvum extract decreases mitochondrial mass and causes injury*

Mitochondria are highly abundant cytoplasmic organelles that play key roles in numerous biochemical processes, including the tricarboxylic acid (TCA) and urea cycles, oxidative phosphorylation, β-oxidation of fatty acids, regulation of intracellular Ca^{2+}levels, and apoptosis signaling (Crompton, 1999). Cardiolipin (CL), a phospholipid, can be found uniquely in the inner membrane of mitochondria. The fluorescent dye 10-N-nonyl-acridine orange (NAO) was used here as a highly specific probe for CL. It is a green fluorescent mitochondrial dye whose staining is independent of mitochondrial membrane potential. NAO binds cardiolipin with higher affinity than other molecules, thereby serving as an indicator of mitochondrial lipid peroxidation and mitochondrial membrane integrity (McMillin and Dowhan, 2002; Petit et al., 1992; Wright et al., 2004). Exposure to *P. parvum* extract led to a

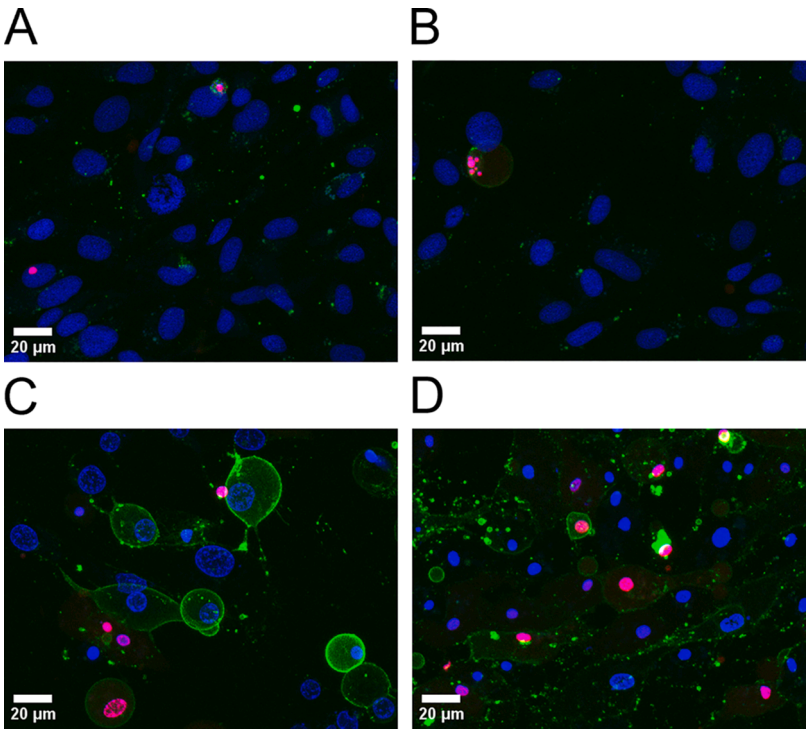

Fig. 4. Annexin V–based detection of apoptotic cells following *P. parvum* extract exposure in RTgill-W1 cells. RTgill-W1 cultures were treated with solvent control (A) or with *P. parvum* extract at sublethal (B), EC_{50} (C), or lethal (D) doses, and followed by 2.5 h incubation. Cells were then stained for 30 min with Hoechst 33342 (blue), Annexin V–FITC (green), and PI (red), and imaged using confocal microscopy.

dose-dependent decrease in NAO fluorescence (Fig. 5) across all tested conditions compared to the solvent control (median=0.91): sublethal (median=0.74), EC_{50} (median=0.36), and lethal (median=0.26).

3.7. Prymnesium parvum extract is associated with lysosomal membrane permeabilization

Mitochondrial membrane alteration can promote oxidative stress, leading to lysosomal membrane permeabilization, and this downstream process likely contributes to the amplification of apoptosis.

The EC_{50} concentration of *P. parvum* extract (Fig. 6E) led to a 46.1 % decrease in LysoTracker Red DND-99 fluorescence in RTgill-W1 cells. The proportion of cells exhibiting low LysoTracker Red staining increased approximately tenfold, from 4.2 % to 44.9 % (Fig. 6F, G).

4. Discussion

Macrolide polyether algal toxins include several structurally and functionally diverse toxin families, each acting through distinct cellular mechanisms. Karlotoxins typically exert cholesterol-dependent membrane permeabilization and pore formation, leading to rapid osmotic imbalance (Place et al., 2024). In contrast, brevetoxins primarily target voltage-gated sodium channels, stabilizing them in an open state and triggering sustained depolarization and calcium influx (Baden et al., 2005). Ichthyotoxins produced by raphidophytes such as *Heterosigma* and *Chattonella* frequently induce pronounced oxidative stress, lipid peroxidation, and ROS-driven cell death (Kim et al., 2000). *Prymnesium* metabolites show evidence of membrane disruption, oxidative stress responses, and ion imbalance, although their precise mechanisms remain less well defined. Taken together, these observations indicate that macrolide polyether algal toxins do not share a single conserved mode of action but instead elicit toxicity through multiple, mechanistically distinct pathways.

Recent mechanistic work on *Karlodinium veneficum* sterolysins has provided detailed insights into sterol-specific pore formation in fish and mammalian membranes (Place et al., 2024; Waters et al., 2015). These studies demonstrate that karlotoxins bind desmethyl sterols with high affinity and form large, poorly selective cationic pores that rapidly dissipate ionic gradients and depolarize membranes. While prymnesins belong to the same broader family of polyether macrolides, their mode of action has not been established at a comparable level of biochemical resolution. Consistent with a complex injury cascade, our cellular endpoints did not reveal a purely membrane-lysis phenotype across concentrations. Rather, organelle-associated stress signatures, including mitochondrial and lysosomal alterations, accompanied the progression toward loss of membrane integrity at higher doses. This phenotype contrasts with the rapid sterol-dependent pore formation and immediate ionic dysregulation reported for karlotoxins (Place et al., 2024; Waters et al., 2015).

The time dependence of *P. parvum* extract-induced cytotoxic effect reported by Varga and Prause (2024), with an approximately twofold higher EC_{50} at 3 h than at 24 h, also argues against an immediate membrane-lytic mechanism and instead supports progressive cellular injury. This temporal sensitivity aligns with our observation of early apoptotic features and progressive organelle dysfunction preceding overt loss of membrane integrity, further distinguishing prymnesin-containing extracts from rapid pore-forming ichthyotoxins.

At present, no mechanistic framework equivalent to the sterol-targeting model established for karlotoxins exists for prymnesins. Our intention here is not to suggest identical pathways, but rather to place our observations within the broader landscape of ichthyotoxin biology. The described dose-dependent transition from early apoptotic features at lower extract concentrations to necrotic membrane failure at higher doses resembles patterns reported for other ichthyotoxins. At the same time, the combined occurrence of early phosphatidylserine externalization, rapid mitochondrial loss, lysosomal alkalinization may represent a mechanistic profile specific to *P. parvum* toxins, likely suggesting a gradual accumulation/distribution of prymnesins in different subcellular compartments. Additional biochemical work with purified prymnesins will be required to understand how sterol-dependent interactions

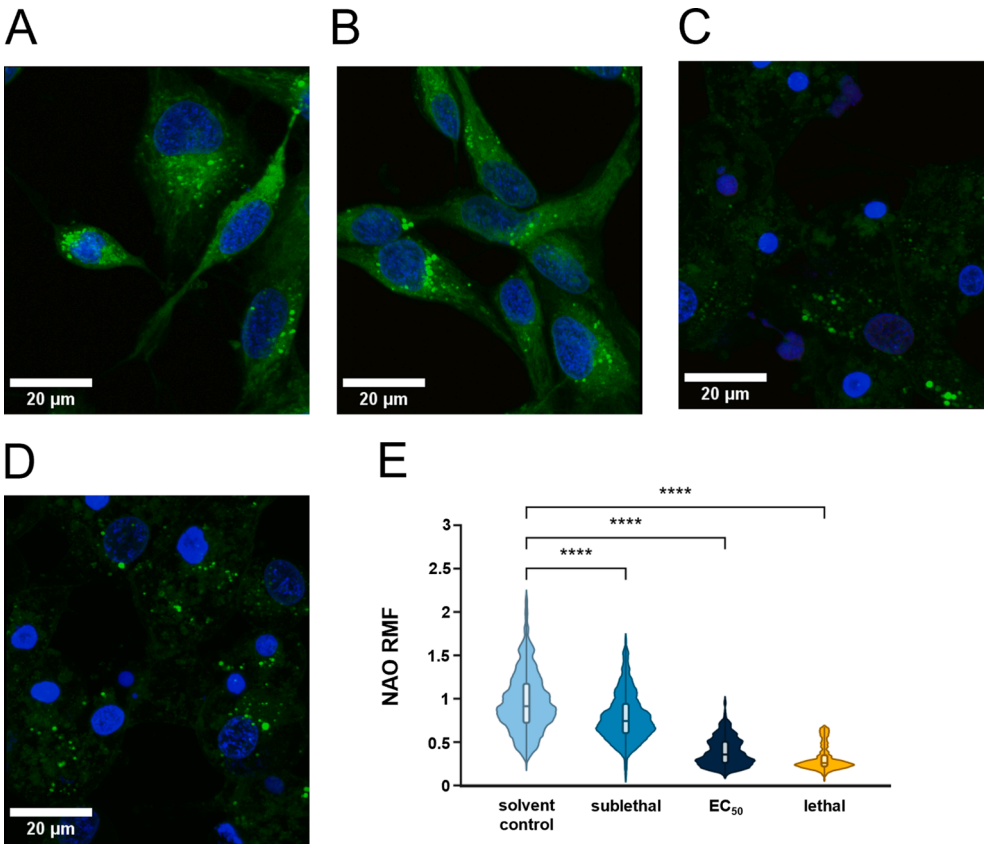

Fig. 5. Effect of *P. parvum* extract on mitochondrial mass in RTgill-W1 cells. RTgill-W1 cultures were dosed with solvent control (A) or with *P. parvum* extract at sublethal (B), EC_{50} (C), or lethal (D) concentrations for 2.5 h. The cell samples were stained for 30 min with Hoechst 33342 (blue) and 10-N-nonyl-acridine orange (NAO, green) and subsequently analyzed by confocal microscopy. The violin plots (E) summarize the statistical analysis of relative mean fluorescence intensity (RMF) for cellular NAO signals. Number of cells analyzed: $n = 945$ (solvent control); $n = 659$ (sublethal); $n = 880$ (EC_{50}); $n = 598$ (lethal). Statistical significance was assessed using the Kruskal–Wallis test followed by Dunn's multiple comparisons test (**** $p < 0.0001$). Created in BioRender. Neer, Z. (2026) https://BioRender.com/zmh8z18.

contribute to these effects.

In this study, we employed a crude methanolic extract rather than purified prymnesins. Although the extract is enriched in B-type prymnesins, it may also contain additional co-metabolites naturally present in bloom material. Using the extract at this stage allows us to capture potentially meaningful synergistic interactions among intracellular components, thereby more closely reflecting the complex toxin mixtures encountered during natural fish-killing events. Targeted testing of purified individual prymnesin congeners represents a logical next step; however, our initial aim was to characterize cellular responses to a biologically realistic mixture of toxins. For this reason, the conclusions of this study are inherently preliminary and will need to be validated using purified toxin preparations.

Beyond simply defining prymnesin-associated toxicity, this study also highlights early, regulated cellular responses at sublethal exposure levels, which are likely to reflect transient stress-adaptation processes that may shape cellular tolerance during harmful algal bloom events (Fig. 7). Dose-dependent cytotoxicity of the *Prymnesium parvum* extract in rainbow trout gill cells has been previously reported and provided the basis for the present study (Varga and Prause et al., 2024). In the present experiments, the EC_{50} concentration was determined using a CTB assay within the first 3–4 h of exposure, serving as a reference point for subsequent analyses. Although the CTB assay indicated a rapid decline in cellular metabolic activity, complementary approaches, including flow cytometry and live-cell imaging, provided greater resolution and revealed that reduced viability was associated with progressive mitochondrial dysfunction and the onset of cell death. To our knowledge, this constellation of cellular events underlying prymnesin-induced injury in fish gill cells has not been reported previously. Together, these findings underscore the utility of multiparametric flow cytometry for resolving early mechanisms of toxicity.

Apoptosis is a regulated form of cell death characterized by distinct morphological features, including chromatin condensation and progressive nuclear compaction (Kerr, 1971). In the present study, increasing concentrations of *Prymnesium parvum* extract induced pronounced nuclear condensation and size reduction in RTgill-W1 cells, consistent with engagement of apoptotic-like processes. A multiparametric approach, combining nuclear morphology, phosphatidylserine externalization, and membrane integrity, revealed a clear, concentration-dependent progression of cellular injury in *Prymnesium parvum* extract–exposed RTgill-W1 cells. At sublethal exposure levels, early apoptotic features predominated, including phosphatidylserine externalization, progressive nuclear condensation, and preserved plasma membrane integrity, supporting the activation of regulated cell death pathways. Quantitative analysis of nuclear morphology demonstrated a shift from intact to compacted nuclei with increasing toxin load, highlighting nuclear structure as a sensitive and reproducible indicator of intracellular stress. With increasing exposure, these apoptotic-like responses progressed to loss of membrane integrity and necrotic outcomes, as evidenced by PI uptake and redistribution of nuclear dyes. Together, these findings indicate that prymnesin-containing extracts induce a gradual cellular response, in which early apoptotic remodeling precedes irreversible membrane failure at higher concentrations, positioning apoptosis as an initial cellular response rather than the terminal outcome of prymnesin toxicity.

The cytotoxicity of *P. parvum* extract was further quantified by its

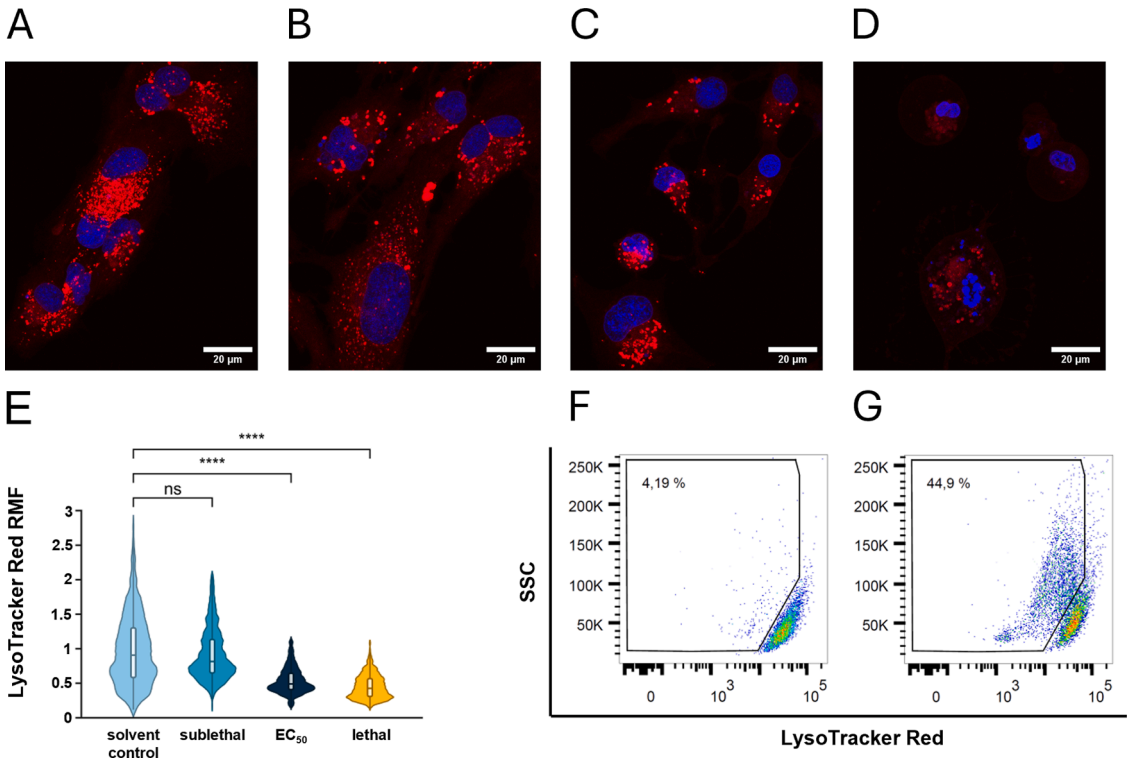

Fig. 6. Effect of *P. parvum* extract on lysosomal activity. RTgill-W1 cultures were treated with solvent control (A) or with *P. parvum* extract at sublethal (B), EC_{50} (C), and lethal (D) doses for 2.5 h, then stained with Hoechst 33342 (blue) and LysoTracker Red DND-99 (red) for 30 min, and analyzed by confocal microscopy. The violin plot (E) summarizes the statistical analysis of confocal microscopy images of the relative mean fluorescence intensity (RMF) of LysoTracker Red DND-99 signals. Number of cells analyzed: $n = 621$ (solvent control); $n = 843$ (sublethal); $n = 604$ (EC_{50}); $n = 501$ (lethal). Statistical significance was determined using the Kruskal–Wallis test followed by Dunn's multiple comparisons test (ns, not significant; **** $p < 0.0001$). Panels (F) and (G) show representative flow cytometry dot plots of RTgill-W1 cells treated with solvent control (F) or the EC_{50} concentration of *P. parvum* extract (G), followed by LysoTracker Red DND-99 staining. SSC: side scatter. Created in BioRender. Neer, Z. (2026) https://BioRender.com/zmh8z18.

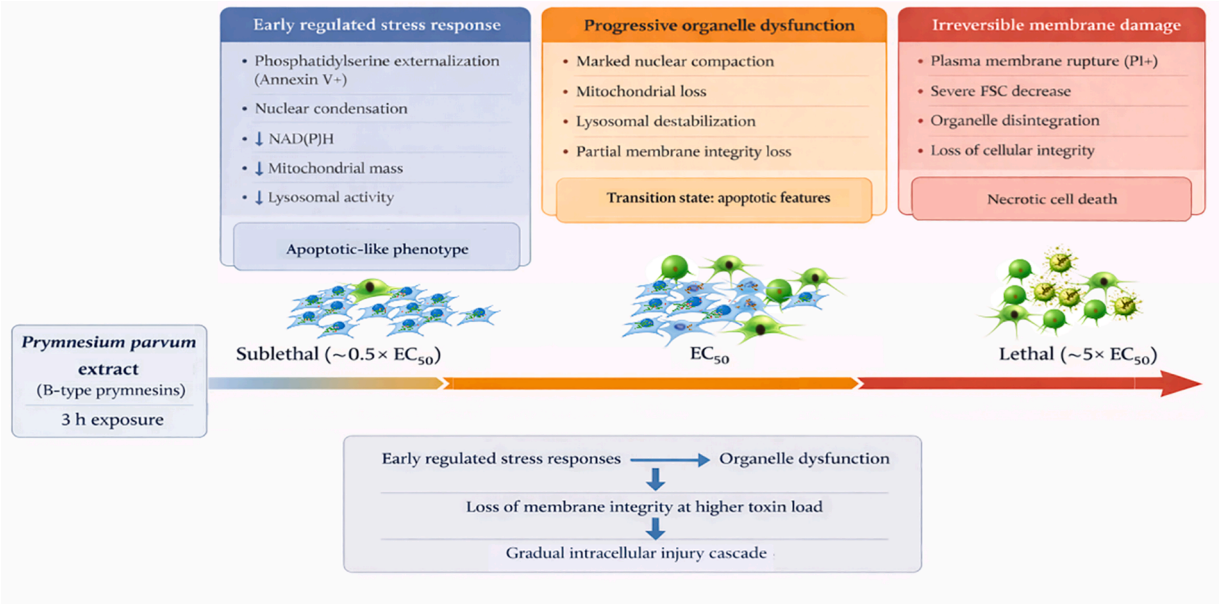

Fig. 7. A summarizing scheme for dose-dependent progression of cellular injury induced by *Prymnesium parvum* extract.

effects on mitochondrial and lysosomal levels. A moderate reduction of the FSC signal and an increase in the SSC signal, both of which are remarkable features of early apoptosis, suggested not only the presence of chromatin condensation, but also of mitochondrial swelling. Mitochondrial impairment could be an "off-target" or a target effect of drugs and contribute to organ toxicities. Mitochondria constantly change shape and size and move inside cells. Disruption of these dynamics can affect mitochondrial function. The centrality of mitochondrial function in eukaryotic cells is reflected in the spectrum of cellular states in which mitochondrial dysfunction manifests (Suomalainen et al., 2024).

Mitochondrial dysfunction was observed as a central feature of *Prymnesium parvum* extract–induced cytotoxicity. Lower mitochondrial membrane mass, accompanied by changes in FSC/SSC parameters, is associated with early apoptotic processes and mitochondrial damage. Cardiolipin plays a critical role in maintaining mitochondrial membrane integrity and cytochrome c association, and its oxidation or loss has been associated with apoptotic signaling pathways (Dudek, 2017). In this context, the observed decrease in cardiolipin-associated fluorescence at lower extract concentrations is consistent with mitochondrial membrane perturbation and could indicate oxidative stress–related injury. Moreover, the loss of NAD(P)H content can occur alongside a decrease in mitochondrial CL content (NAO fluorescence), a pattern consistent with mitochondrial membrane lipid peroxidation (Shao et al., 2010). The sensitivity of trout gill epithelial cells to prymnesins may be due to their limited capacity to eliminate reactive oxygen species via cellular antioxidant pathways (Shao et al., 2008). While these findings suggest mitochondrial involvement in prymnesin-induced cell death, direct assessment of mitochondrial membrane potential, network integrity, and ROS generation was beyond the scope of the present study and need to be addressed in future work.

Lysosomes play an important modulatory role in cell death pathways, primarily by amplifying intracellular injury rather than initiating cell death. In the present study, lysosomal function was markedly affected by exposure to *Prymnesium parvum* extract, as evidenced by significantly reduced lysosomal staining in fluorescence microscopy and flow cytometry at increasing toxin concentrations. This decrease is consistent with lysosomal dysfunction and suggests impaired catalytic activity. Together with the observed mitochondrial alterations, these findings indicate that prymnesin-containing extracts induce coordinated organelle-level stress responses that contribute to the progression of cellular injury.

Although several ichthyotoxins exhibit ROS- and caspase-dependent mechanisms, such pathways have not been established for prymnesins yet. In connection with the present study, no caspase activation was detected at the 3-hour endpoint (data not shown), suggesting that caspase involvement, if it is present, may be temporally separated from the early cellular responses observed here and should be addressed in future kinetic studies to reveal further mechanistic details of prymnesin-induced biological effects in gill epithelial cells.

The observed concentration-dependent progression from early apoptotic features, including phosphatidylserine externalization and nuclear condensation, toward mitochondrial and lysosomal dysfunction and loss of membrane integrity indicates a graded pattern of cellular injury. While the specific molecular targets and pathways involved remain unresolved, these findings place prymnesin-containing extracts within the broader context of ichthyotoxin-induced cellular stress responses rather than defining a discrete mode of action. The results presented here, therefore, serve as a framework for future studies employing purified prymnesin congeners to further clarify the mechanisms underlying *P. parvum*–associated fish toxicity.

Cells exposed for 3 h to B-type prymnesins from *Prymnesium parvum* exhibit a gradual response depending on toxin concentration. At sublethal doses, cells display an early regulated stress response characterized by nuclear condensation, reduced NAD(P)H levels, decreased mitochondrial mass, and diminished lysosomal activity, consistent with an apoptotic-like phenotype. Notably, phosphatidylserine externalization becomes progressively more pronounced with increasing toxin concentration, indicating a concentration-dependent amplification of membrane asymmetry loss. At EC_{50} concentration, progressive organelle dysfunction becomes evident, including marked nuclear compaction, mitochondrial loss, lysosomal destabilization, and partial loss of membrane integrity, representing a transition state with apoptotic features. At lethal concentrations, irreversible plasma membrane rupture (PI^+), severe forward scatter (FSC) decrease, organelle disintegration, and complete loss of cellular integrity are observed, consistent with necrotic cell death. Overall, increasing toxin load drives a continuum from early regulated stress responses to organelle dysfunction and ultimately membrane failure, reflecting a gradual intracellular injury cascade.

5. Conclusions

In summary, *P. parvum* extract induces injury to cultured rainbow trout gill cells, characterized by coordinated nuclear, mitochondrial, and lysosomal dysfunction leading to cell death. Specifically, the EC_{50} concentration of the *P. parvum* extract induced substantial alterations in cellular morphology, nuclear condensation, and exposure of the cell surface to phosphatidylserine (PS), consistent with the early stages of apoptosis. The resulting cell death occurs at concentrations observed during bloom events. The effect of multiple or chronic exposures to *P. parvum* extracts, which may be even more relevant to environmental exposures, was not assessed. Furthermore, our studies suggest that measuring redox-associated alterations (NAD(P)H decrease) alongside mitochondrial injury can help evaluate the sublethal effects of prymnesins in fish and other species. In this regard, using flow cytometry-based analyses and sensitive fluorescent probes as markers of cell injury in aquatic species is valuable for broader applications in aquatic toxicology.

Funding

This research was funded in whole or in part by the Austrian Science Fund (FWF) [grant DOI:10.55776/I5707]. For open access purposes, the author has applied a CC BY public copyright license to any author accepted manuscript version arising from this submission. The project on which this manuscript is based was partly funded by the German Federal Ministry of Education and Research (BMBF) within the Research Initiative for the Conservation of Biodiversity (FEdA) under the funding code 16LW0561k. Zsuzsanna Neer received a stipend from the Eötvös Loránd University. Tamás Felföldi was supported by the National Multidisciplinary Laboratory for Climate Change project (RRF-2.3.1–21–2022–00014) under Hungary's National Recovery and Resilience Plan, funded by the European Union's Recovery and Resilience Facility. The responsibility for the content of this publication lies with the authors. Open access funding was provided by the University of Veterinary Medicine Vienna.

CRediT authorship contribution statement

Zsuzsanna Neer: Writing – review & editing, Writing – original draft, Visualization, Methodology, Investigation, Formal analysis, Data curation, Conceptualization. **Endre Kiss:** Writing – review & editing, Methodology, Formal analysis, Data curation. **Urban Tillmann:** Writing – review & editing, Resources, Methodology. **Magdalena Pöchhacker:** Writing – review & editing, Methodology. **Balázs Vajna:** Writing – review & editing, Resources. **Tamás Felföldi:** Writing – review & editing, Resources. **János Matkó:** Writing – review & editing, Methodology, Conceptualization. **Elisabeth Varga:** Writing – review & editing, Supervision, Resources, Project administration, Funding acquisition, Conceptualization.

Declaration of competing interest

The authors declare the following financial interests/personal relationships which may be considered as potential competing interests:

Elisabeth Varga reports financial support was provided by Austrian Science Fund. Zsuzsanna Neer reports financial support was provided by Eötvös Loránd University. Elisabeth Varga and Urban Tillmann reports financial support was provided by the German Federal Ministry of Education and Research (BMBF). Tamas Felfoeldi reports financial support was provided by Hungary's National Recovery and Resilience Plan. Urban Tillmann reports that he is a member of the Editorial Advisory Board of Harmful Algae. If there are other authors, they declare

that they have no known competing financial interests or personal relationships that could have appeared to influence the work reported in this paper.

Acknowledgements

The RTgill-W1 cell line was obtained from Kristin Schirmer, Department of Environmental Toxicology, EAWAG – Swiss Federal Institute of Aquatic Science and Technology, Dübendorf, Switzerland. This research was supported using resources of the VetCore Facility (Mass Spectrometry & Imaging) of the University of Veterinary Medicine Vienna and the Max Perutz Labs BioOptics FACS Facility, Vienna. We thank Dr. Ursula Reichart for her continuous support and helpful discussions, which significantly improved the quality of our research. This paper is the result of research conducted within the Interuniversity Research Platform for Agrobiotechnology Tulln (IFA-Tulln) by BOKU-University, vetmeduni Vienna and TU Wien.

Supplementary materials

Supplementary material associated with this article can be found, in the online version, at doi:10.1016/j.hal.2026.103112.

Data availability

Data will be made available on request.

References

Baden, D.G., Bourdelais, A.J., Jacocks, H., Michelliza, S., Naar, J., 2005. Natural and derivative brevetoxins: historical background, multiplicity, and effects. Env. Health Perspect 113, 621–625. https://doi.org/10.1289/ehp.7499.

Baker, J.W., Grover, J.P., Brooks, B.W., Ureña-Boeck, F., Roelke, D.L., Errera, R., Kiesling, R.L., 2007. Growth and toxicity of *Prymnesium parvum* (Haptophyta) as a function of salinity, light, and temperature. J. Phycol. 43, 219–227. https://doi.org/10.1111/j.1529-8817.2007.00323.x.

Berger, R., Liaaen-Jensen, S., McAlister, V., Guillard, R.R.L., 1977. Carotenoids of prymnesiophyceae (Haptophyceae). Biochem. Syst. Ecol. 5, 71–75. https://doi.org/10.1016/0305-1978(77)90034-5.

Bertin, M.J., Zimba, P.V., Beauchesne, K.R., Huncik, K.M., Moeller, P.D.R., 2012. Identification of toxic fatty acid amides isolated from the harmful alga *Prymnesium parvum* Carter. Harmful. Algae 20, 111–116. https://doi.org/10.1016/j.hal.2012.08.005.

Binzer, S.B., Svenssen, D.K., Daugbjerg, N., Alves-de-Souza, C., Pinto, E., Hansen, P.J., Larsen, T.O., Varga, E., 2019. A-, B-, and C-type prymnesins are clade-specific compounds and chemotaxonomic markers in *Prymnesium parvum*. Harmful. Algae 81, 10–17. https://doi.org/10.1016/j.hal.2018.11.010.

Bols, N.C., Barlian, A., Chirino-Trejo, M., Caldwell, S.J., Goegan, P., Lee, L.E.J., 1994. Development of a cell line from primary cultures of rainbow trout, *Oncorhynchus mykiss* (Walbaum), gills. J. Fish. Dis. 17, 601–611. https://doi.org/10.1111/j.1365-2761.1994.tb00258.x.

Cano, M., del, V., Reyes, J.M., Park, C.Y., Gao, X., Mori, K., Chuck, R.S., Gehlbach, P.L., 2008. Demonstration by redox fluorometry that sulforaphane protects retinal pigment epithelial cells against oxidative stress. Invest. Ophthalmol. Vis. Sci. 49, 2606–2612. https://doi.org/10.1167/iovs.07-0960.

Chen, X., Liu, S., Ding, Q., Teame, T., Yang, Y., Ran, C., Zhang, Z., Zhou, Z., 2023. Research advances in the structure, function, and regulation of the gill barrier in teleost fish. Water Biol. Secur. 2, 100139. https://doi.org/10.1016/j.watbs.2023.100139.

Crompton, M., 1999. The mitochondrial permeability transition pore and its role in cell death. Biochem. J. 341, 233–249. https://doi.org/10.1042/bj3410233.

Dafni, Z., Ulitzur, S., Shilo, M., 1972. Influence of light and phosphate on toxin production and growth of *Prymnesium parvum*. J. Gen. Microbiol. 70, 199–207. https://doi.org/10.1099/00221287-70-2-199.

Dai, Y., Yang, S., Zhao, D., Hu, C., Xu, W., Anderson, D.M., Li, Y., Song, X.P., Boyce, D.G., Gibson, L., Zheng, C., Feng, L., 2023. Coastal phytoplankton blooms have expanded and intensified in the 21st century. Nature 615, 280–284. https://doi.org/10.1038/s41586-023-05760-y.

Darzynkiewicz, Z., Bruno, S., Del Bino, G., Gorczyca, W., Hotz, M.A., Lassota, P., Traganos, F., 1992. Features of apoptotic cells measured by flow cytometry. Cytometry 13. https://doi.org/10.1002/cyto.990130802.

Dudek, J., 2017. Role of cardiolipin in mitochondrial signaling pathways. Front. Cell Dev. Biol. 5. https://doi.org/10.3389/fcell.2017.00090.

Edvardsen, B., Eikrem, W., Throndsen, J., Sáez, A.G., Probert, I., Medlin, L.K., 2011. Ribosomal DNA phylogenies and a morphological revision provide the basis for a revised taxonomy of the Prymnesiales (Haptophyta). Eur. J. Phycol. 46, 202–228. https://doi.org/10.1080/09670262.2011.594095.

Edvardsen, B., Paasche, E., 1998. Bloom dynamics and physiology of prymnesium and chrysomulina. In book: physiological ecology of harmful algal blooms. In: NATO ASI Series G, 41. Publisher: Springer-Verlag, pp. 193–208.

Feng, L., Wang, Y., Hou, X., Qin, B., Kutser, T., Qu, F., Chen, N., Paerl, H.W., Zheng, C., 2024. Harmful algal blooms in inland waters. Nat Rev Earth Env. 5, 631–644. https://doi.org/10.1038/s43017-024-00578-2.

Fistarol, G., Legrand, C., Granéli, E., 2003. Allelopathic effect of *Prymnesium parvum* on a natural plankton community. Mar. Ecol. Prog. Ser. 255, 115–125. https://doi.org/10.3354/meps255115.

Gobler, C.J., 2020. Climate change and harmful algal blooms: insights and perspective. Harmful. Algae 91, 101731. https://doi.org/10.1016/j.hal.2019.101731.

Granéli, E., Hansen, P.J., 2006. Allelopathy in harmful algae: a mechanism to compete for resources? Ecology of Harmful Algae. Springer Berlin Heidelberg, pp. 189–201. https://doi.org/10.1007/978-3-540-32210-8_15.

Granéli, E., Salomon, P.S., 2010. Factors influencing allelopathy and toxicity in *Prymnesium parvum* 1. JAWRA J. Am. Water Resour. Assoc. 46, 108–120. https://doi.org/10.1111/j.1752-1688.2009.00395.x.

Granéli, E., Edvardsen, B., Roelke, D.L., Hagström, J.A., 2012. The ecophysiology and bloom dynamics of *Prymnesium* spp. Harmful. Algae 14, 260–270. https://doi.org/10.1016/j.hal.2011.10.024.

Griffith, A.W., Gobler, C.J., 2020. Harmful algal blooms: a climate change co-stressor in marine and freshwater ecosystems. Harmful. Algae 91, 101590. https://doi.org/10.1016/J.HAL.2019.03.008.

Hallegraeff, G.M., 1993. A review of harmful algal blooms and their apparent global increase. Phycologia 32, 79–99. https://doi.org/10.2216/i0031-8884-32-2-79.1.

Häder, D.P., Banaszak, A.T., Villafañe, V.E., Narvarte, M.A., González, R.A., Helbling, E.W., 2020. Anthropogenic pollution of aquatic ecosystems: emerging problems with global implications. Sci. Total. Environ. 713, 136586. https://doi.org/10.1016/j.scitotenv.2020.136586.

Henrikson, J.C., Gharfeh, M.S., Easton, A.C., Easton, J.D., Glenn, K.L., Shadfan, M., Mooberry, S.L., Hambright, K.D., Cichewicz, R.H., 2010. Reassessing the ichthyotoxin profile of cultured *Prymnesium parvum* (golden algae) and comparing it to samples collected from recent freshwater bloom and fish kill events in North America. Toxicon. 55, 1396–1404. https://doi.org/10.1016/j.toxicon.2010.02.017.

Hill, B.N., Saari, G.N., Steele, W.B., Corrales, J., Brooks, B.W., 2020. Nutrients and salinity influence *Prymnesium parvum* (UTEX LB 2797) elicited sublethal toxicity in Pimephales promelas and Danio rerio. Harmful. Algae 93, 101795. https://doi.org/10.1016/j.hal.2020.101795.

Igarashi, T., Oshima, Y., Murata, M., Yasumoto, T., 1995. Chemical Studies On Prymnesins Isolated from *Prymnesium Parvum*. Harmful Marine Algal Blooms.

Igarashi, T., Satake, M., Yasumoto, T., 1996. Prymnesin-2: a potent ichthyotoxic and hemolytic glycoside isolated from the red tide alga *Prymnesium parvum*. J. Am. Chem. Soc. 118, 479–480. https://doi.org/10.1021/ja9534112.

Igarashi, T., Satake, M., Yasumoto, T., 1999. Structures and partial stereochemical assignments for prymnesin-1 and prymnesin-2: potent hemolytic and ichthyotoxic glycosides isolated from the red tide alga *Prymnesium parvum*. J. Am. Chem. Soc. 121, 8499–8511. https://doi.org/10.1021/ja991740e.

Keller, M.D., Selvin, R.C., Claus, W., Guillard, R.R.L., 1987. Media for the culture of oceanic ultraphytoplankton 1,2. J. Phycol. 23, 633–638. https://doi.org/10.1111/j.1529-8817.1987.tb04217.x.

Kerr, J.F.R., 1971. Shrinkage necrosis: a distinct mode of cellular death. J. Pathol. 105, 13–20. https://doi.org/10.1002/path.1711050103.

Kim, D., Oda, T., Ishimatsu, A., Muramatsu, T., 2000. Galacturonic-acid-induced increase of superoxide production in red tide phytoplankton Chattonella marina and Heterosigma akashiwo. Biosci. Biotechnol. Biochem. 64, 911–914. https://doi.org/10.1271/bbb.64.911.

Kozakai, H., Oshima, Y., Yasumoto, T., 1982. Isolation and structural elucidation of hemolysin from the phytoflagellate *Prymnesium parvum*. Agric. Biol. Chem. 46, 233–236. https://doi.org/10.1271/bbb1961.46.233.

Köhler, J., Varga, E., Spahr, S., Gessner, J., Stelzer, K., Brandt, G., Mahecha, M.D., Kraemer, G., Pusch, M., Wolter, C., Monaghan, M.T., Stöck, M., Goldhammer, T., 2024. Unpredicted ecosystem response to compound human impacts in a European river. Sci. Rep. 14, 16445. https://doi.org/10.1038/s41598-024-66943-9.

Laing, R.A., Fischbarg, J., Chance, B., 1980. Noninvasive measurements of pyridine nucleotide fluorescence from the cornea. Invest. Ophthalmol. Vis. Sci. 19, 96–102.

Legrand, C., Rengefors, K., Fistarol, G.O., Granéli, E., 2003. Allelopathy in phytoplankton - biochemical, ecological and evolutionary aspects. Phycologia 42, 406–419. https://doi.org/10.2216/i0031-8884-42-4-406.1.

Liebert, F., Deerns, W.M., 1920. Onderzoek naar de oorzaak van een vischsterfte in den polder Workumer-Nieuwland, nabij Workum. Rijksintituut voor Visscherijonderzoek. Verh. rapp. 81–93.

Masters, B.R., Ghosh, A.K., Wilson, J., Matschinsky, F.M., 1989. Pyridine nucleotides and phosphorylation potential of rabbit corneal epithelium and endothelium. Invest. Ophthalmol. Vis. Sci. 30, 861–868.

McKim, J., Schmieder, P., Veith, G., 1985. Absorption dynamics of organic chemical transport across trout gills as related to octanol-water partition coefficient. Toxicol. Appl. Pharmacol. 77, 1–10. https://doi.org/10.1016/0041-008X(85)90262-5.

McMillin, J.B., Dowhan, W., 2002. Cardiolipin and apoptosis. Biochim. Biophys. Acta (BBA) - Mol. Cell Biol. Lipids 1585, 97–107. https://doi.org/10.1016/S1388-1981(02)00329-3.

Minet, O., Beuthan, J., Mildažiene, V., Baniene, R., 2004. Fluorescence techniques in biomedicine: from the monitoring of cell metabolism to image processing in cancer detection. Reviews in Fluorescence 2004. Springer US, Boston, MA, pp. 195–219. https://doi.org/10.1007/978-0-306-48672-2_10.

Paerl, H.W., Huisman, J., 2009. Climate change: a catalyst for global expansion of harmful cyanobacterial blooms. Env. Microbiol Rep 1, 27–37. https://doi.org/10.1111/j.1758-2229.2008.00004.x.

Petit, J., Maftah, A., Ratinaud, M., Julien, R., 1992. 10 N-nonyl acridine orange interacts with cardiolipin and allows the quantification of this phospholipid in isolated mitochondria. Eur. J. Biochem. 209, 267–273. https://doi.org/10.1111/j.1432-1033.1992.tb17285.x.

Place, A.R., Ramos-Franco, J., Waters, A.L., Peng, J., Hamann, M.T., 2024. Sterolysin from a 1950s culture of *Karlodinium veneficum* (aka *Gymnodinium veneficum* Ballantine) forms lethal sterol dependent membrane pores. Sci. Rep. 14, 17998. https://doi.org/10.1038/s41598-024-68669-0.

Pozarowski, P., Grabarek, J., Darzynkiewicz, Z., 2003. Flow Cytometry of Apoptosis, Chapter 7. Curr Protoc Cytom. https://doi.org/10.1002/0471142956.cy0719s25. Unit 7.19.

Rasmussen, S., Meier, S., Gedsted Andersen, N., Blossom, H., Øllgaard Duus, J., Fog Nielsen, K., Ostenfeld Larsen, T., 2016. Chemodiversity of the ladder-frame prymnesin polyethers of the fish-killing microalgal *Prymnesium parvum*. Planta Med. 81, S1–S381. https://doi.org/10.1055/s-0036-1596109.

Remmel, E.J., Hambright, K.D., 2012. Toxin-assisted micropredation: experimental evidence shows that contact micropredation rather than exotoxicity is the role of *Prymnesium* toxins. Ecol. Lett. 15, 126–132. https://doi.org/10.1111/j.1461-0248.2011.01718.x.

Roelke, D., Errera, R., Kiesling, R., Brooks, B., Grover, J., Schwierzke, L., Ureña-Boeck, F., Baker, J., Pinckney, J., 2007. Effects of nutrient enrichment on *Prymnesium parvum* population dynamics and toxicity: results from field experiments, Lake Possum Kingdom, USA. Aquat. Microb. Ecol. 46, 125–140. https://doi.org/10.3354/ame046125.

Roelke, D.L., Grover, J.P., Brooks, B.W., Joanglass, Davidbuzan, Southard, G.M., Lorainefries Gable, G.M., Schwierzke-Wade, L., Meridithbyrd, Janetnelson, 2011. A decade of fish-killing prymnesium parvum blooms in Texas: roles of in flow and salinity. J. Plankton. Res. 33, 243–253. https://doi.org/10.1093/plankt/fbq079.

Schirmer, K., Chan, A.G.J., Greenberg, B.M., Dixon, D.G., Bols, N.C., 1997. Methodology for demonstrating and measuring the photocytotoxicity of fluoranthene to fish cells in culture. Toxicol. Vitro 11, 107–119. https://doi.org/10.1016/S0887-2333(97)00002-7.

Sales, C.F., Santos, K.P.E.dos, Rizzo, E., Ribeiro, R.I.M.de A., Santos, H.B.dos, Thomé, R. G., 2017. Proliferation, survival and cell death in fish gills remodeling: from injury to recovery. Fish. Shellfish. Immunol. 68, 10–18. https://doi.org/10.1016/j.fsi.2017.07.001.

Shao, J., Eckert, M.L., Lee, L.E.J., Gallagher, E.P., 2008. Comparative oxygen radical formation and toxicity of BDE 47 in rainbow trout cell lines. Mar Env. Res 66, 7–8. https://doi.org/10.1016/j.marenvres.2008.02.007.

Shao, J., Dabrowski, M.J., White, C.C., Kavanagh, T.J., Gallagher, E.P., 2010. Flow cytometric analysis of BDE 47 mediated injury to rainbow trout gill epithelial cells. Aquat. Toxicol. 97, 42–50. https://doi.org/10.1016/j.aquatox.2009.11.013.

Southard, G.M., Fries, L.T., Barkoh, A., 2010. *Prymnesium parvum*: the Texas experience. JAWRA J. Am. Water Resour. Assoc. 46, 14–23. https://doi.org/10.1111/j.1752-1688.2009.00387.x.

Suomalainen, A., Nunnari, J., 2024. Mitochondria at the crossroads of health and disease. Cell. https://doi.org/10.1016/j.cell.2024.04.037.

Svenssen, D.K., Binzer, S.B., Medić, N., Hansen, P.J., Larsen, T.O., Varga, E., 2019. Development of an indirect quantitation method to assess ichthyotoxic B-type prymnesins from *Prymnesium parvum*. Toxins. (Basel) 11, 251. https://doi.org/10.3390/toxins11050251.

Tillmann, U., 2003. Kill and eat your predator: a winning strategy of the planktonic flagellate *Prymnesium parvum*. Aquat. Microb. Ecol. 32, 73–84. https://doi.org/10.3354/ame032073.

Tomer, A., Harker, L.A., Burstein, S.A., 1988. Flow cytometric analysis of normal human megakaryocytes. Blood 71. https://doi.org/10.1182/blood.v71.5.1244.bloodjournal7151244.

van Genderen, H., Kenis, H., Lux, P., Ungeth, L., Maassen, C., Deckers, N., Narula, J., Hofstra, L., Reutelingsperger, C., 2006. *In vitro* measurement of cell death with the annexin A5 affinity assay. Nat. Protoc. 1, 363–367. https://doi.org/10.1038/nprot.2006.55.

Varga, E., Prause, H.C., Riepl, M., Hochmayr, N., Berk, D., Attakpah, E., Kiss, E., Medić, N., Del Favero, G., Larsen, T.O., Hansen, P.J., Marko, D., 2024. Cytotoxicity of *Prymnesium parvum* extracts and prymnesin analogs on epithelial fish gill cells RTgill-W1 and the human colon cell line HCEC-1CT. Arch. Toxicol. 98, 999–1014. https://doi.org/10.1007/s00204-023-03663-5.

Waters, A.L., Oh, J., Place, A.R., Hamann, M.T., 2015. Stereochemical studies of the karlotoxin class using NMR spectroscopy and DP4 chemical-shift analysis: insights into their mechanism of action. Angew. Chem. 127, 15931–15936. https://doi.org/10.1002/ange.201507418.

Wood, C.M., Kelly, S.P., Zhou, B., Fletcher, M., O'Donnell, M., Eletti, B., Pärt, P., 2002. Cultured gill epithelia as models for the freshwater fish gill. Biochim. Biophys. Acta (BBA) - Biomembr. 1566, 72–83. https://doi.org/10.1016/S0005-2736(02)00595-3.

Wright, M.M., Howe, A.G., Zaremberg, V., 2004. Cell membranes and apoptosis: role of cardiolipin, phosphatidylcholine, and anticancer lipid analogues. Biochem. Cell Biol. 82, 18–26. https://doi.org/10.1139/o03-092.

Zhitomirsky, B., Farber, H., Assaraf, Y.G., 2018. LysoTracker and MitoTracker Red are transport substrates of P-glycoprotein: implications for anticancer drug design evading multidrug resistance. J. Cell Mol. Med. 22 (4), 2131–2141. https://doi.org/10.1111/jcmm.13485.

Zhou, B., Liu, C., Wang, J., Lam, P.K.S., Wu, R.S.S., 2006. Primary cultured cells as sensitive *in vitro* model for assessment of toxicants-comparison to hepatocytes and gill epithelia. Aquat. Toxicol. 80, 109–118. https://doi.org/10.1016/j.aquatox.2006.07.021.